Journal of Contaminant Hydrology 181 (2015) 161–171

Contents lists available at ScienceDirect

Journal of Contaminant Hydrology

journal homepage: www.elsevier.com/locate/jconhyd

Colloid release and clogging in porous media: Effects of solution ionic strength and flow velocity

Saeed Torkzaban [a,*], Scott A. Bradford [b], Joanne L. Vanderzalm [a], Bradley M. Patterson [c,d], Brett Harris [e], Henning Prommer [c,f,g]

[a] CSIRO Land and Water, Glen Osmond, SA 5064, Australia
[b] US Salinity Laboratory, USDA, ARS, Riverside, CA, United States
[c] CSIRO Land and Water, Floreat Park, Western Australia, Australia
[d] School of Chemistry and Biochemistry, The University of Western Australia, Crawley 6009, Australia
[e] Curtin University, Dept. Exploration Geophysics, Dick Perry Ave, 6151, Perth, WA 6151, Australia
[f] School of Earth and Environment, The University of Western Australia, Crawley 6009, Australia
[g] National Centre for Groundwater Research and Training, Flinders University, Adelaide, GPO Box 2100, SA 5001, Australia

ARTICLE INFO

Article history:
Received 12 February 2015
Received in revised form 5 June 2015
Accepted 14 June 2015
Available online 19 June 2015

Keywords:
Release
In-situ colloids
Clogging
Permeability
Modeling

ABSTRACT

The release and retention of in-situ colloids in aquifers play an important role in the sustainable operation of managed aquifer recharge (MAR) schemes. The processes of colloid release, retention, and associated permeability changes in consolidated aquifer sediments were studied by displacing native groundwater with reverse osmosis-treated (RO) water at various flow velocities. Significant amounts of colloid release occurred when: (i) the native groundwater was displaced by RO-water with a low ionic strength (IS), and (ii) the flow velocity was increased in a stepwise manner. The amount of colloid release and associated permeability reduction upon RO-water injection depended on the initial clay content of the core. The concentration of released colloids was relatively low and the permeability reduction was negligible for the core sample with a low clay content of about 1.3%. In contrast, core samples with about 6 and 7.5% clay content exhibited: (i) close to two orders of magnitude increase in effluent colloid concentration and (ii) more than 65% permeability reduction. Incremental improvement in the core permeability was achieved when the flow velocity increased, whereas a short flow interruption provided a considerable increase in the core permeability. This dependence of colloid release and permeability changes on flow velocity and colloid concentration was consistent with colloid retention and release at pore constrictions due to the mechanism of hydrodynamic bridging. A mathematical model was formulated to describe the processes of colloid release, transport, retention at pore constrictions, and subsequent permeability changes. Our experimental and modeling results indicated that only a small fraction of the in-situ colloids was released for any given change in the IS or flow velocity. Comparison of the fitted and experimentally measured effluent colloid concentrations and associated changes in the core permeability showed good agreement, indicating that the essential physics were accurately captured by the model.

1. Introduction

Aquifer sediments always contain a certain amount of colloidal particles (e.g., clay and silica) deposited on the grain surfaces. Understanding of the mechanisms controlling the release and transport of in-situ colloids in natural porous media is required for numerous applications, including enhanced oil recovery, regeneration of filter beds, erosion of earthen embankments, and managed aquifer recharge (MAR) (Goldenberg et al., 1984; Khilar and Fogler, 1984; Konikow et al., 2001; Zeinijahromi et al., 2011). Colloids are

* Corresponding author. Tel.: +61 883038491.
E-mail address: Saeed.Torkzaban@csiro.au (S. Torkzaban).

http://dx.doi.org/10.1016/j.jconhyd.2015.06.005
0169-7722/

usually immobile during native groundwater conditions. However, they may be released into the groundwater in response to perturbations of the native conditions, such as the injection of water with a different chemical composition or varying flow rates (Bradford et al., 2015a; Grolimund et al., 2001; Rosenbrand et al., 2012; Tosco et al., 2009). The released colloids are transported with flowing water and may subsequently re-deposit down gradient (e.g., at pore constrictions), resulting in permeability reduction of the porous medium, commonly referred to as clogging (e.g., Mays and Hunt, 2005; Ochi and Vernoux, 1998).

Clogging has been recognized to be the most significant technical challenge in MAR operations and is attributed to a combination of physical, chemical and biological processes (Martin, 2013). Commonly, the assessment of physical clogging in MAR has focused on the effect of colloids present in the source water through a measure of the Membrane Filtration Index (Dillon et al., 2001; Pavelic et al., 2007). However, when advanced treatment such as reverse osmosis results in source water for recharge with a low ionic strength (IS), the corresponding changes in solution chemistry (decrease in IS) raise the potential for clogging via in-situ colloid release and transport. Emerging large-scale applications of MAR in Australia involve well injection of low IS source water (e.g., domestic wastewater and industrial wastewater produced during coal seam gas recovery) into sandstone aquifers (Seibert et al., 2014). In addition, when well injection techniques are utilized for recharge, there can be considerable spatial and temporal variability in flow rate due to the applied injection pressure, periods of intermittent flow and periodic surging or back-washing to remediate near-well clogging. Therefore, a comprehensive understanding of colloid release, retention, and clogging is needed for efficient design and successful operation of a wide variety of environmental and engineering applications, including MAR.

Previous research has conclusively shown that colloid release from a collector surface depends on the relative strengths of the resisting adhesive torque and force, the applied hydrodynamic torque, and the diffusive force (Bergendahl and Grasso, 2000; Shen et al., 2007; Torkzaban et al., 2007, 2012; Vasiliadou and Chrysikopoulos, 2011). Therefore, the process of colloid release is expected to depend on the chemical conditions of the aqueous (pH, IS, and ionic composition) and solid phases, because of their influence on the resisting adhesive torque and force. Many attempts have been made to describe experimental observations of colloid release within the framework of the Derjaguin, Landau, Verwey, and Overbeek (DLVO) theory (Derjaguin and Landau, 1941; Verwey and Overbeek, 1948), in which the colloid interaction energy is quantified as the sum of van der Waals and electrostatic interactions. However, numerous deviations from classical DLVO predictions have been reported, especially in the presence of multivalent salts (Grosberg et al., 2002; Sasidharan et al., 2014; Torkzaban et al., 2013). For example, it has often been observed that only a fraction of deposited colloids on grain surfaces is released by lowering the IS at which the colloid interaction energies are predicted by the DLVO theory to be highly repulsive (e.g., Shen et al., 2012; Torkzaban et al., 2013). Consequently, the colloid release process cannot be simulated by employing a simple first-order kinetic rate unless the total releasable colloid mass is also determined and adjusted in the model (Bradford et al., 2012, 2015b; Roy and Dzombak, 1996). It should be mentioned that some attempts have been made to resolve the discrepancies between DLVO predictions and observed release behavior by considering non-DLVO forces (e.g., Lewis acid–base interactions and Born repulsion) and the influence of nano-scale physical and/or chemical heterogeneities on colloid and grain surfaces (Bradford and Torkzaban, 2012, 2013; Duffadar and Davis, 2007; Shen et al., 2012).

The rate and amount of colloid release with changes in flow velocity have been reported to exhibit more complex behavior than that induced by changes in solution chemistry. For example, Bradford et al. (2012) reported little colloid release with increasing flow velocity, while Bedrikovetsky et al. (2012) showed a greater dependency of colloid release on flow velocity. Furthermore, colloid release induced by increasing flow velocity has been reported as both rapid (Bergendahl and Grasso, 2000; Ryan and Elimelech, 1996) and slow (Ochi and Vernoux, 1998). In principle, a balance of hydrodynamic and adhesive torques and forces can be used to determine the amount of colloid release for a given change in the flow velocity (Bergendahl and Grasso, 2000). However, it is now well accepted that values of hydrodynamic and adhesive torques and forces are spatially distributed in porous media because of nano- and micro-scale surface roughness, chemical heterogeneities, and pore-scale velocity distributions (Bradford et al., 2011, 2014; Shen et al., 2012). Furthermore, colloids that are weakly associated with grain surfaces in a secondary energy minimum are expected to be more sensitive to hydrodynamic forces than those associated with a strong primary energy minimum. These weakly associated colloids can be translated across grain surfaces by hydrodynamic forces until they become retained on the surface or released into the bulk solution (Kuznar and Elimelech, 2007; Torkzaban et al., 2010). This process is expected to influence the kinetics of colloid release induced by a change in the flow velocity.

Once the colloids are released into the bulk solution and are transported in the porous medium, solution chemistry and hydrodynamic conditions influence their subsequent interactions with grain surfaces affecting their re-deposition (Grolimund et al., 1998; Mondal and Sleep, 2012; Zhou et al., 2009). While colloid attachment on grain surfaces is unlikely following their release by chemical changes, straining processes such as retention at locations with larger surface roughness and grain–grain contacts, size exclusion, and hydrodynamic bridging may still be important. It should be mentioned, however, that retention at rough locations on grain surfaces and grain–grain contacts may depend on adhesive interactions, and is not a purely mechanical process (Blume et al., 2002; Bradford et al., 2013). Hydrodynamic bridging refers to the process in which multiple colloids, whose individual size is much smaller than the size of the pore constriction, simultaneously arrive and are captured at a pore constriction (Ramachandran and Fogler, 1999). Bridging is a complex process that depends on the colloid concentration, hydrodynamic forces, and the size of the colloid and pore constriction (Bacchin et al., 2013; Ramachandran et al., 2000). Size exclusion refers to the colloid retention at a pore constriction that is smaller in size than the colloid (Bradford and Torkzaban, 2013). Hydrodynamic bridging and size exclusion can both cause severe and rapid clogging (i.e., permeability reduction) in porous media, whereas retention

on grain surfaces, roughness locations, and grain–grain contacts are expected to have a minimal influence on permeability alterations. The effects of flow velocity on hydrodynamic bridging and its implications for colloid release and clogging are still poorly understood and warrant further studies.

In this paper we examined the effects of solution IS and flow rate on the processes of colloid release, transport, and the resultant clogging potential in sandstone aquifer samples. The range of applied experimental conditions is relevant to MAR via well injection that introduce a low salinity source water into a sandstone aquifer hosting a mixed-salt groundwater. Effluent colloid concentrations and overall core permeability were measured during the experiments. Specifically, we address: (i) the influence of reducing IS on the amount and kinetics of colloid release in a mixed salt system; (ii) the effect of varying flow velocity, encompassing near-well injection rates, sequential increases in velocity, and flow interruption, on colloid release and clogging behavior; and (iii) the development of a suitable mathematical model to describe colloid release, retention, and associated permeability changes consistent with the observed colloidal release and transport processes.

2. Material and methods

2.1. Injected water and aquifer materials

The experiments were conducted using three consolidated (sandstone) core samples from different depths of the Yarragadee Formation within the Perth Basin of Western Australia. The Yarragadee Formations form a thick expansive aquifer, consisting of interbedded sandstone, siltstone and shale (Salama, 2005). It is an important water resource for Western Australia and in particular the people of Perth City.

Characterization of the aquifer material included particle size (<2 mm) and quantitative X-ray diffraction (XRD) analysis. The cores consisted primarily of sand with a mean particle size of 0.18 mm and a coefficient of uniformity (D_{60}/D_{10}, where 60% and 10% of the mass are finer than D_{60} and D_{10}, respectively) of 2.14. The quantitative XRD analysis showed that quartz (SiO_2) was the dominant mineral, with small amount of kaolinite, mica, smectite, and feldspar minerals (see Table 1). The clay fraction was determined to be 7.4% and 6.1% of the bulk material for core samples taken from depths 466 and 555 m below ground level (mBGL) respectively, and lower at 1.3% for the core sample from 391 mBGL. Scanning electron microscopy (SEM) with energy dispersive X-ray microbeam (EDX) analysis showed that sand grains were partially covered with clay minerals with typical morphologies of kaolinite (data not shown).

Table 1
Properties of the core samples used in the clogging study.

Sample depth (mBGL)	391	466	555
Components	Quartz (89%) Kaolinite (1.3%) Feldspar (10%)	Quartz (77%) Kaolinite (7.4%) Feldspar (15%)	Quartz (75%) Kaolinite (6.1%) Feldspar (17%)
Porosity (%)	32	29	28
Initial hydraulic conductivity (m/day)	2.3	0.20	0.22
Dispersivity (cm)	0.01	0.01	0.01

Groundwater from the Yarragadee aquifer was filtered through a 0.45 m membrane to remove suspended colloids and used to vacuum-saturate and precondition the cores. Negligible colloid release was observed during the saturation and preconditioning phases. Water from a double reverse-osmosis filter, hereafter denoted as RO-water, was used in the colloid release experiments. The electrical conductivity (EC) of the RO-water was less than 0.5 mS/m, sodium and calcium concentrations were below 1 mg/L and its pH was 5.8. Salinity and major ions in the Yarragadee groundwater at the location where the cores were collected were low, but still in excess of those in RO-water. The EC, sodium and calcium concentrations and pH of this groundwater were 35 mS/m, 47 mg/L and 9 mg/L and 7.5, respectively.

2.2. Experimental setup and procedure

The experimental setup included a Hassler coreholder, water reservoir, HPLC pump, fraction collector, pressure transmitter, and a data acquisition system. Fig. 1 schematically shows the experimental setup that was operated in a constant temperature laboratory (20 ± 1 °C). The dimensions of the core sample were 3.8 cm in diameter and 7 cm in length. A confining pressure of 50 bar was applied over the rubber sleeve containing the core plug during the tests. Differential-pressure transmitters were used to measure the pressure values across the core plug. The values of pressure difference were measured over the course of the experiment. The pressure data was used to calculate the permeability from the one dimensional form of Darcy's Law for laminar flow through porous media. The outlet pressure was always atmospheric.

The sequence of influent solutions and flow rates for each experiment are described below and summarized in Table 2. Initially, the core was preconditioned by flushing with about 20 pore volumes (PVs) of groundwater during which the pressure difference across the core was measured to determine the initial hydraulic conductivity (K_0). In this step, a conservative tracer (1 mM $NaNO_3$) was added to the groundwater for a period of 2 PVs to determine the porosity and dispersivity of the core sample. Nitrate breakthrough concentrations were measured using a UV/vis spectrophotometer at a wavelength of 210 nm. The average pore water velocity (v) during the preconditioning step was 8 m day^{-1}. Subsequently, solution IS was reduced by displacing native groundwater with RO-water at v of either 8 or 30 m day^{-1} (Step A). Following the completion of Step A, the flow rate was sequentially and incrementally increased (Steps B1–B5) from 2 to 100 mL min^{-1}, corresponding to Reynolds number in the range of 0.002–0.13, which confirmed that the laminar flow condition was satisfied. The pulse duration and v of each step in the experiment are given in Table 2. An additional step (Step C) was applied to one of the core sample in which, following the phase with a flow rate of 100 mL min^{-1}, the flow was stopped for 2 min and then resumed at a flow rate of 7 mL min^{-1} for several PVs. This step was conducted to examine the effect of flow interruption on the permeability change of the core.

At the outlet of the coreholder, effluent samples were collected using a fraction collector at specified time intervals

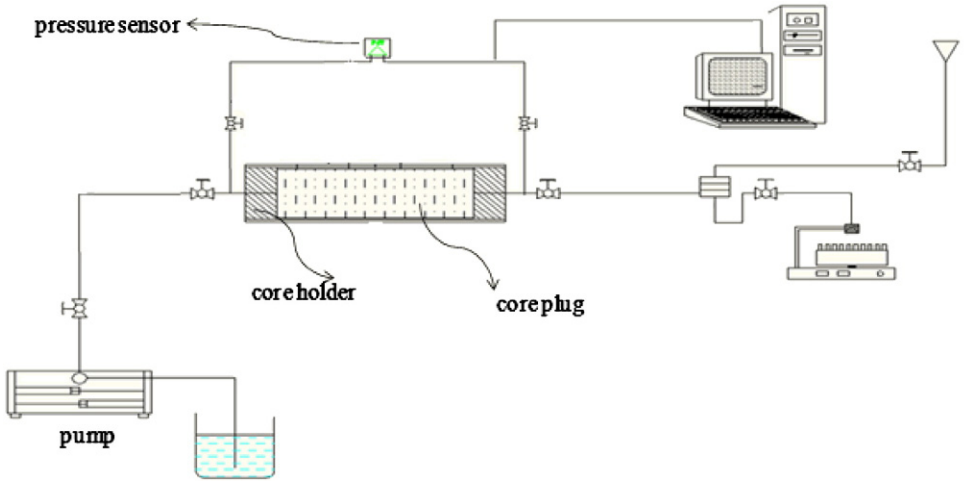

Fig. 1. Experimental set-up for colloid release and clogging experiments.

and analyzed for colloid concentration using a UV/vis spectrophotometer at a wavelength of 600 nm. A linear correlation was established between the absorbance readings (optical density) and colloid concentrations following a procedure described by Grolimund et al. (1996). This correlation was verified to be independent of the solution chemistry and flow rates for our experimental conditions. The colloid size distribution in the effluent suspension was periodically measured using a dynamic light scattering (DLS) method. Permeability changes were assessed using the normalized hydraulic conductivity (K/K_0), e.g., the ratio of the overall hydraulic conductivity (K) of the core at any given time to the initial hydraulic conductivity (K_0) determined during the injection of the native groundwater, versus the number of pore volumes of injected water.

Table 2
Summary of the conditions used in the three core-flooding experiments.

Step	Starting pore volume	Flow rate (ml/min)	Average pore water velocity (m/d)	Solution
Core sample 391				
Precondition	<0	2	8	NGW
A	0	2	8	RO
B1	24.6	7	29	RO
B2	40	14	58	RO
B3	48	36	150	RO
B4	64	50	208	RO
B5	77.5	100	416	RO
Core sample 555				
Precondition	<0			NGW
A	0	7	30	RO
B1	34	14	59	RO
B2	56	36	170	RO
B3	79	50	236	RO
B4	102	100	472	RO
Core sample 466				
Precondition	<0			NGW
A	0	7	30	RO
B1	32.5	14	59	RO
B2	57	36	153	RO
B3	81	50	212	RO
B4	104	100	424	RO
C	130[a]	7	30	RO

NGW = native groundwater; RO = reverse osmosis water.
[a] Indicates the time at which the flow was interrupted for 2 min.

2.3. Conceptual and mathematical model

Our conceptual model for colloid release, retention, and subsequent clogging is illustrated in Fig. 2. Colloidal particles are assumed to be initially deposited on grain surfaces. Upon a change in chemical or hydrodynamic conditions, a fraction of colloids may be released into the aqueous phase due to alteration of adhesive or hydrodynamic forces or by a combination of these factors. Following release, the suspended colloids are transported through the porous medium with the flow. Re-attachment to grain surfaces (pore walls) is assumed to be unlikely because conditions are highly unfavorable for attachment in the presence of RO-water. However, conditions may be favorable for colloid bridging at pore constrictions (i.e., hydrodynamic bridging) depending on the pore size, flow velocity, and suspended colloid concentration and size distribution. It is expected that hydrodynamic bridging will cause severe permeability reductions. Furthermore, it is assumed that excessive flow velocity may cause liberation (breaking) of some of the colloid bridges at pore constrictions, leading to a sharp increase of permeability.

The mathematical model developed to account for these conceptual processes incorporates three mass balance equations to describe the processes of colloid transport, release, and retention. An additional equation was incorporated to describe the permeability reduction caused by colloid retention at pore constrictions.

Chemical changes (e.g., IS, pH, and cation exchange) often take place within normality fronts traveling through the porous medium (Grolimund and Borkovec, 2006). The travel velocity of a chromatographic front approaches that of a conservative tracer in porous media with a low cation exchange capacity. In this work, the IS was determined from

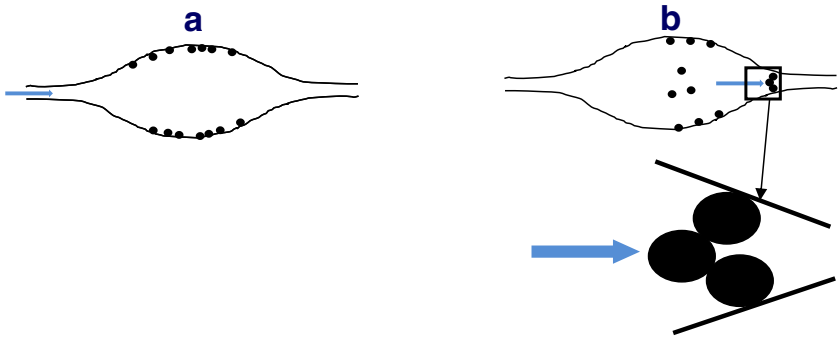

Fig. 2. A conceptual illustration of pore body and throats in porous media. (a) shows that at equilibrium all the colloidal particles are attached to the pore surface. (b) shows that a fraction of the colloids are released and bridged at the pore constrictions following the release of colloids.

the solution of the mass balance equation for a conservative 1:1 electrolyte tracer (e.g., chloride ion) as:

$$\frac{\partial nC_{IS}}{\partial t} = \frac{\partial J_{IS}}{\partial x} \tag{1}$$

where n [−] is the porosity, x [L] is the distance in the direction of flow, and t [T] is the time, C_{IS} [$M_s L^{-3}$; M_s denotes the mass] is the tracer concentration in the aqueous phase, and J_{IS} [$M_s L^{-2} T^{-1}$] is the ion flux (sum of the advection and dispersion flux).

Colloid transport was described using the standard advection–dispersion equation with terms for colloid release from the matrix of the porous media and retention at pore constrictions:

$$\frac{\partial C}{\partial t} = D\frac{\partial^2 C}{\partial x^2} - v\frac{\partial C}{\partial x} - \frac{r_{rel}}{n} - \frac{r_{ret}}{n} \tag{2}$$

where C [$M_c L^{-3}$, where M_c is mass of colloids] is the colloid concentration in the aqueous phase, D [$L^2 T^{-1}$] is the hydrodynamic dispersion coefficient, v [LT^{-1}] is the average pore water velocity, r_{rel} [$M_c L^{-3} T^{-1}$] is the release rate from pore walls, and r_{ret} [$M_c L^{-3} T^{-1}$] is the retention rate at pore constrictions.

The release process needs to be coupled with the solution IS during Step A of the experiments. The process of colloid release from grain surfaces (pore walls) into the aqueous phase was modeled using a single first-order kinetic equation accounting for the total releasable mass of colloids upon a change in IS (Bradford et al., 2012):

$$\rho_b \frac{\partial S_1}{\partial t} = r_{rel} = -\kappa_1 \rho_b (S_1 - f_{nr1} S_{i1}) H_0 (S_1 - f_{nr1} S_{i1}) \tag{3}$$

where S_1 [M_c/M] is the colloid concentration on grain surfaces, ρ_b [ML^{-3}] is the bulk density of porous media, κ_1 [T^{-1}] is the release rate constant, S_{i1} [M_c/M] is the initial colloid concentration on grain surfaces, f_{nr1} [−] is the fraction of colloid deposit that is not released with a given change in the solution IS, and $H_0(S_1 - f_{nr1}S_{i1})$ is the Heaviside function that is equal to 1 when $S_1 > f_{nr1}S_{i1}$ and 0 when $S_1 \le f_{nr1}S_{i1}$. The term f_{nr1} is a function of solution IS. We assume that colloid release only begins when IS decreases below a critical value (C_{ISc}) and f_{nr1} is described using a step function (e.g., Khilar and Fogler, 1984; Kia et al., 1987). Eq. (3) was also used to describe colloid release induced by changes in the flow rate. In this case, f_{nr1} is the fraction of colloid deposit that was not released with a change in flow rate. The amount of colloid release with chemical and hydrodynamic alterations is equal to $(1 - f_{nr1})S_{i1}$. Note that re-attachment of the released colloids was not considered in Eq. (3) because conditions are unfavorable for attachment during the release phase.

The following mass balance equation was used to describe processes of colloid retention and release at the pore constrictions:

$$\rho_b \frac{\partial S_2}{\partial t} = r_{ret} = \lambda n C\left(1 - \frac{S_2}{S_{max2}}\right) - \kappa_2 \rho_b (S_2 - f_{nr2} S_{i2}) H_0 (S_2 - f_{nr2} S_{i2}) \tag{4}$$

where S_2 [$M_c M^{-1}$] is the colloid concentration at the pore constrictions, S_{max2} [$M_c M^{-1}$] is the maximum concentration of colloids retained at the pore constrictions, S_{i2} [$M_c M^{-1}$] is the initial colloid concentration at the pore constrictions, λ [T^{-1}] is the retention coefficient, f_{nr2} [−] is the fraction of retained colloids that was not released with a change in the flow rate, and κ_2 [T^{-1}] is the release rate constant. In analogy to colloid filtration theory (Yao et al., 1971), a simple first-order expression with respect to the concentration of suspended colloids was used to account for the rate of colloid capture at pore constrictions (first term on right hand side of Eq. (4)). Note that a Langmuirian blocking model was employed to account for filling of retention sites at pore constrictions (Adamczyk et al., 1995). Release is modeled in a similar fashion to Eq. (3), but with a separate functional dependency of f_{nr2} on v.

It is expected that colloid retention at pore constrictions will cause severe permeability reduction. In this work we employed an empirical equation to relate S_2 at pore constrictions to permeability changes (Khilar and Fogler, 1998):

$$\frac{K}{K_0} = \frac{1}{1 + \beta S_2} \tag{5}$$

where β [−] is commonly referred to as formation damage (clogging) factor. The secondary influence of S_2 on porosity was considered to be minor and not accounted for in the model.

The governing equations for the conservative tracer, colloid transport, release, retention, and permeability changes were implemented and solved using COMSOL Multiphysics software (COMSOL, Inc., Palo Alto, CA 94301). For the simulation discussed below, a zero flux boundary condition was used at the inlet, and a concentration gradient of zero was specified at the outlet. An initial condition of no suspended colloids in solution and a fixed uniform concentration of initially deposited colloids in the simulation domain were used. The Levenberg–Marquardt algorithm in the Optimization Module of COMSOL was employed to estimate the values of model parameters by fitting the measured colloid concentrations in the outlet of the core and average core permeability to the solution of the governing equations.

Values of porosity and dispersivity were estimated by fitting the tracer (NO_3^-) breakthrough concentrations to the solution of Eq. (1). The value for dispersivity was found to be very low (~0.01 cm), confirming that the core was rather homogeneous. Note that the effect of clogging on the possible changes of dispersivity was not considered in this study. The average pore water velocity (v) was calculated from the porosity and direct measurements of the flow rate. The initial value of S_{i1} of each core sample was estimated based on the XRD analysis of the clay content (see Table 3), whereas the initial value of S_{i2} was set to zero. Values of S_{i1} and S_{i2} for each subsequent release step (B1–B5) were obtained directly from the model output. A critical parameter in modeling colloid release was to determine the fraction of colloid release as a result of temporal changes in solution IS and flow velocity. Experimental information on the initial clay content and mass balance of the effluent colloid concentration during each release step was used to constrain the optimization of f_{nr1}. This approach assumes that the amount of retained colloids at pore constrictions was much less than that of in the effluent. The values of other parameters such as κ_1, λ, β, S_{max2}, and κ_2 were determined by fitting the solution of Eqs. (2)–(5) to colloid release curves and permeability data. However, not all of these parameters were fitted during each release step. For example, only κ_1, f_{nr1}, λ and S_{max2} were determined during Step A when colloid release was induced by lowering IS to that of RO water. It should be mentioned that potential effect of gravity force on the kinetics of colloid release and retention was not considered in the present study. This effect has recently been shown to be significant for colloid transport under different velocities and ionic strengths, especially for the larger and denser particles (Chrysikopoulos and Syngouna, 2014).

Table 3
Summary of the values of the parameters of the best fit for modeling of the three core-flooding experiments.

Flow velocity (m/d)	κ_1 (s^{-1})	$1-f_{nr1}$	$1-f_{nr2}$	κ_2 (s^{-1})	λ (s^{-1})	β	R^2 %
Core sample 391: S_{i1} (g_c/kg) = 10, S_{max2} (g_c/kg) = 2							
8	0.000125	0.053	NA	NA	0.002	NA	96
29	0.0007	0.0085	0.09	0.012	NA	NA	97
58	0.002	0.005	0.01	0.02	NA	NA	94
150	0.003	0.009	0.24	0.045	NA	NA	95
208	0.004	0.005	0.04	0.055	NA	NA	96
416	0.006	0.025	0.45	0.07	NA	NA	94
Core sample 555: S_{i1} (g_c/kg) = 50, S_{max2} (g_c/kg) = 0.6							
30	0.00055	0.156	NA	NA	0.009	2.5	98
59	0.00065	0.027	0.4	0.09	NA	2.7	96
153	0.0026	0.018	0.66	0.25	NA	3.0	98
212	0.0042	0.01	0.45	0.3	NA	3.2	98
424	0.012	0.011	0.7	0.5	NA	3.8	99
Core sample 466: S_{i1} (g_c/kg) = 50, S_{max2} (g_c/kg) = 2.2							
30	0.0004	0.16	NA	NA	0.0021	2.5	96
59	0.00065	0.05	0.3	0.038	NA	2.5	95
153	0.0023	0.045	0.4	0.16	NA	2.9	97
212	0.005	0.02	0.2	0.2	NA	3.1	98
424	0.0085	0.03	0.83	0.3	NA	5.1	97

NA — denotes not applicable.

3. Results and discussion

Three core samples from different depths (391, 466, and 555 mBGL) of the Yarragadee aquifer were selected to examine the effects of changes in IS and flow velocities on the processes of colloid release and clogging. Figs. 3, 4, and 5 present measured (symbols) and simulated (solid lines) colloid release concentration data (effluent concentrations versus pore volumes) obtained from core samples 391, 555, and 466, respectively. Figs. 4 and 5 also present permeability changes over the course of experiments with core samples 466 and 555. As it will be discussed later in the paper, there was no reduction in permeability during the experiment with core sample 391.

3.1. Impact of IS reduction

Figs. 3–5 illustrate that a step decrease in the IS during Step A resulted in the release of colloid deposits on grain surfaces of the aquifer materials. The released colloids were transported through the porous media and appeared in the core effluent after about one PV. The colloid concentration sharply increased and reached a maximum after around 2 or 3 PVs, and then gradually decreased with time. It took about 25 PVs for the colloid concentration to drop to around 15% of the peak concentration. Note that a greater amount of colloid was released during Step A from core samples 466 and 555, than 391. This is attributed to the greater initial clay content of cores 466 and 555 (6.1–7.4%), compared to that of core 391 (1.3%).

Changes in the solution chemistry (e.g., IS decrease) induce colloid release by altering colloid–colloid and colloid–collector interaction energies (e.g., Ryan and Elimelech, 1996). The net interaction energy between surfaces is commonly described using DLVO theory. Many examples of colloid release with IS reduction can be found in the literature (Ryan and Elimelech, 1996). Most of these studies show that a decrease in IS below a critical value leads to colloid release due to reduction or elimination of the secondary energy minimum (Ryan and Gschwend, 1994; Syngouna and Chrysikopoulos, 2015; Torkzaban et al., 2010). Note that classical DLVO theory predicts an infinitely deep primary minimum, implying that the likelihood of colloid release is virtually zero by alteration of chemical conditions. However, inclusion of short-range repulsive forces such as Born and hydration interactions and the influence of nanoscale physical heterogeneity (roughness) produce a primary minimum of finite depth (Bradford and Torkzaban, 2013; Shen et al., 2012). Colloid release from a primary energy minimum with changes in solution chemistry may therefore be possible depending on the

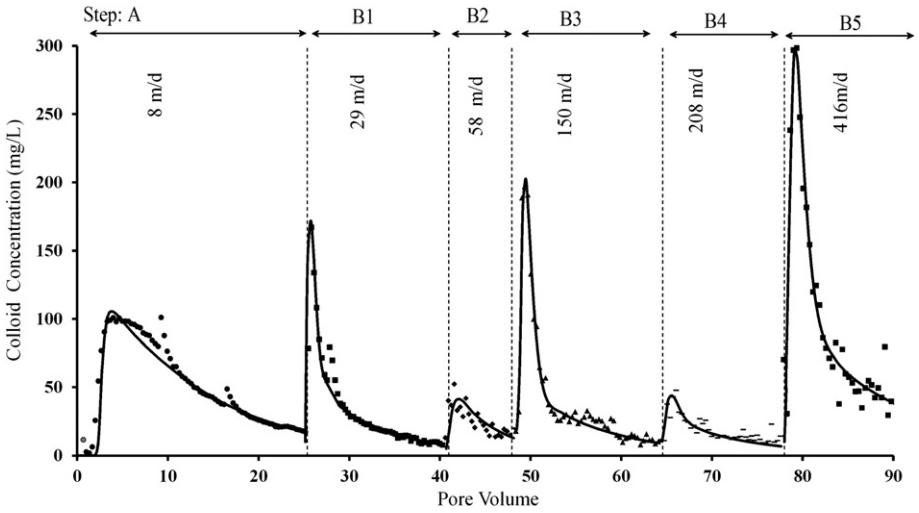

Fig. 3. Experimental data (symbols) and model calculations (solid lines) for colloid release behavior of the core sample 391. No reduction in permeability was evident.

depth of primary minimum and the height of energy barrier (Bradford et al., 2015a; Shen et al., 2012).

The colloid mass balance for Step A, as shown in Figs. 3–5, revealed that only a small fraction (<16%) of the in situ colloid deposit was released when IS decreased by switching to RO water. This observation may suggest that the released colloids were held in a secondary minimum or a shallow primary minimum in the presence of native groundwater, and were subsequently released when the IS was lowered upon injection of RO water. The rate of colloid release is primarily controlled by the rate of colloid diffusion and the thickness of diffusion boundary layer when the adhesive energy minimum is eliminated (Ryan and Gschwend, 1994). Apparently, the majority (>84%) of the in situ colloids on sediment grains were held in a deep primary energy minimum in the presence of native groundwater, and therefore were not released upon IS reduction. The results indicate that the magnitude of energy barrier to detachment was much greater than the average thermal energy possessed by the colloids (~1.5 kT) when the IS was lowered to that of RO water. However, DLVO calculations in which Born repulsion was incorporated showed no energy barrier against detachment upon injection of RO water (data not shown). This discrepancy could be attributed to the influence of nanoscale chemical heterogeneity on the colloid surfaces on the interaction energies. It is known that adsorbed multivalent cations, such as Ca^{2+}, can create nanoscale chemical heterogeneity on colloid surfaces that can neutralize or reverse the surface charge at specific locations (Grosberg et al., 2002; Roy and Dzombak, 1996; Torkzaban et al., 2013). It has been demonstrated that when mineral surfaces (e.g., clay) exhibit selectivity for a particular cation, the exchange of that cation for a lower selectivity cation will occur only when the less selective ion is present at high concentrations (Roy and Dzombak, 1996; Torkzaban et al., 2013).

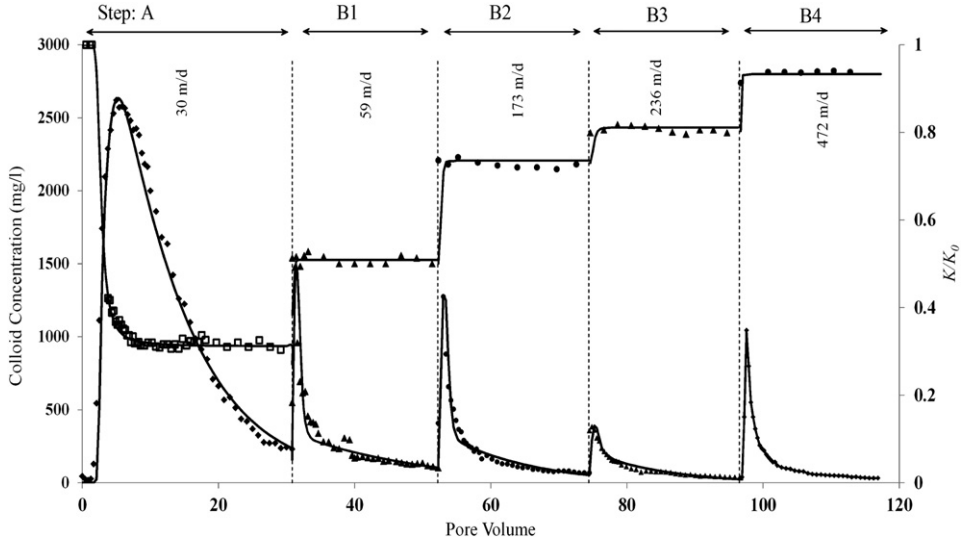

Fig. 4. Experimental data (symbols) and model calculations (solid lines) for colloid release behavior and permeability response of the core sample 555 to reduction in water salinity and increase in water velocity.

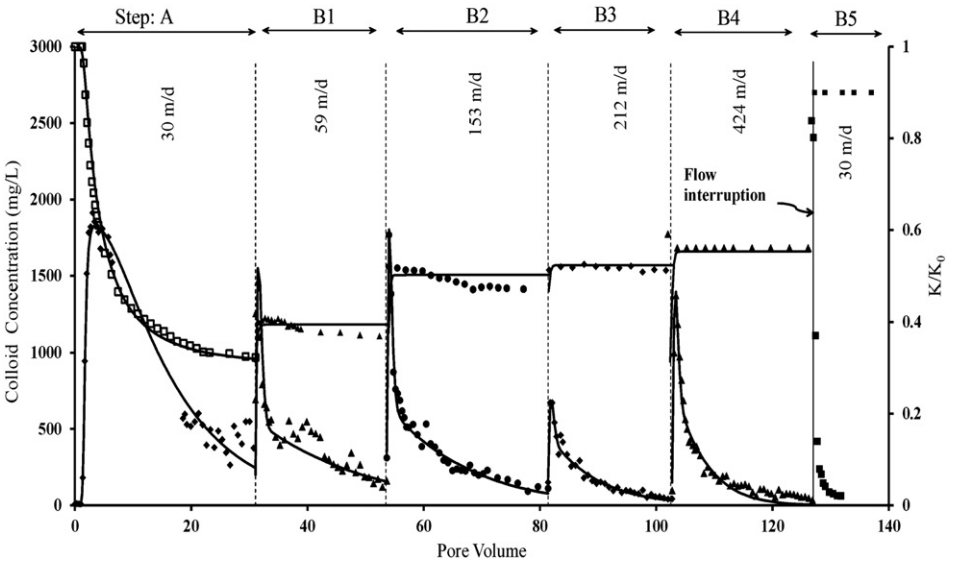

Fig. 5. Experimental data (symbols) and model calculations (solid lines) for colloid release behavior and permeability response of the core sample 466 to reduction in water salinity and increase in water velocity.

The initial hydraulic conductivity of core samples 391, 466, and 555 in the presence of native groundwater was about 2.3, 0.20, and 0.22 m/d, respectively, with a coefficient of variation of 3%. The pressure difference across core sample 391 did not show a noticeable increase after injection of RO water. This indicates that colloid release during Step A (Fig. 3) had a negligible impact on the permeability of core 391 that had a relatively small amount of clay (~1.3%). Conversely, the average permeability of the core significantly decreased by about 65% when RO-water was injected into cores 466 and 555 that had a larger amount of clay (~6–7%). The permeability reduction was most pronounced during the first few PVs and then gradually leveled off with further injection of RO water. The significant and sudden clogging during the first few PVs in Step A of cores 466 and 555 implies that the clogging process was highly dependent on the colloid concentration in the aqueous phase and the initial hydraulic conductivity. Peak effluent colloid concentrations for cores 466 (~2600 mg/L) and 555 (~1700 mg/L) were much higher than core 391 (~100 mg/L). Furthermore, K_0 was much smaller for cores 466 and 555 (0.2–0.22 m day^{-1}) than core 391 (2.3 m day^{-1}). These observations suggest that the high concentration of released colloids and smaller mean pore sizes in cores 466 and 555 compared to those of core 391 caused colloid retention and clogging at pore constrictions. The concentration of colloids and the pore size distribution of the porous medium are expected to play an important role in colloid bridging at the pore constrictions (Mays and Hunt, 2005; Wiesner et al., 1996). As discussed later, we suggest that hydrodynamic bridging at the pore constrictions was the principal mechanism of colloid retention and subsequent permeability reduction (cf., Fig. 2).

3.2. Impact of velocity changes

Following the completion of Step A, the average pore water velocity (v) was increased in stepwise fashion (Steps B1–B5) in order to examine the effect of hydrodynamic forces on colloid release and permeability of the cores. For example, in core sample 391 the value of v was successively increased from 8 to 29, 58, 150, and 208, and eventually 416 m/day. Figs. 3–5 show that a step increase in v led to substantial amounts of colloid release in all three core samples. For each step increase in v the colloid release behavior exhibited a sharp peak followed by slow release over many PVs (~15 PVs). These results demonstrate the profound effect of flow velocity on in-situ colloid release. Representative analysis of the size distribution of the released colloids in each step showed that the average hydrodynamic radii of the colloids were about 1–3 m and remained constant (within the experimental errors) during the course of experiment. We, therefore, conclude that properties of the released colloids were almost constant, in spite of the fact that there was a finite amount of colloids that could be released at each v level. It should be mentioned that we did not observe any noticeable colloid release when the pore-water velocity was increased up to 100 m/day during the preconditioning phase when the native groundwater was being injected into the cores. This insensitivity of colloid release to velocity in the presence of native groundwater can be explained by the increase in the adhesive force at higher IS.

Colloid mass balance information for each step increase in v revealed that only a small fraction of the total colloid deposit on grain surfaces was released upon each increase in flow velocity. This fraction was exhausted over the course of experimental phase associated with a specific v. This behavior can be attributed to alteration of torque and force balances acting on colloids on grain surfaces upon each step increase in v. Colloid release is expected to increase with an increase in v due to an increase in the hydrodynamic shear force and the associated increase in the applied hydrodynamic torque which can overcome the resisting adhesive torque (Bergendahl and Grasso, 2000; Bradford et al., 2013). It is evident that there exists a critical hydrodynamic shear force above which only a fraction of deposited colloids on sand grains was released. This can be attributed to the spatial

variations in hydrodynamic forces due to pore structures and roughness, the location of deposited colloids on sand grains, and differences in the strength of adhesive interactions for deposited colloids.

Figs. 4 and 5 indicate that the sharp increase in colloid release upon an increase in v resulted in an increase in the average permeability of core samples 555 and 446. For example, the value of K/K_0 in core sample 555 sharply increased from 0.3 to 0.44, when v was increased from 30 to 59 m/d and then remained constant at this same v. Subsequent increases in v from 59 to 170, 236, and 472 m/day resulted in a considerable increase in the permeability. Note that the final permeability was about 86% of the initial value when v was increased to 472 m/d. Similarly, the permeability of core sample 466 suddenly increased to about 40% of its original value when v was increased from 30 to 59 m/day. Subsequent stepwise increases in the flow velocity from 59 to 153, 212, and 424 m/day resulted in an analogous increase in the permeability. Comparison of Figs. 4 and 5 reveals that the extent of improvement in permeability with an increase in v was smaller in core sample 466 than in 555, suggesting the important effect of pore-size distribution on permeability changes.

The observed dependence of permeability on v (Figs. 4 and 5) may be explained by the mechanism of hydrodynamic bridging (Fig. 2). Multiple colloids may form a bridge across a pore constriction and cause pore blockage (Ramachandran et al., 2000). Bridging requires the simultaneous arrival of multiple colloids at a pore constriction and hydrodynamic forces to push colloids against the pore entrance (Ramachandran and Fogler, 1999). Hydrodynamic bridging is, therefore, expected to be sensitive to the colloid concentration as demonstrated in Step A of Figs. 3–5, the hydrodynamic conditions, and the pore-size distribution (Bacchin et al., 2013).

Flow interruptions are expected to eliminate the pore blockage due to hydrodynamic bridging during which the entrapped colloids may freely diffuse in and out of the pore constriction. An additional experiment was conducted to test this hypothesis. For core 466 which had shown limited recovery in permeability in response to increasing velocity, the flow was stopped for about 2 min after continuously injection of about 135 PVs of RO water. It is observed in Fig. 5 that the normalized hydraulic conductivity substantially increased from 0.58 to 0.9 when the flow was resumed at a v of 30 m/day. Moreover, a very high peak of released colloids was observed following the flow interruption.

The above observations provide convincing evidence for the role of hydrodynamic bridging at pore constrictions on permeability changes in Figs. 4 and 5. Consequently, the observed increase in permeability with an increase in v indicates that colloids retained at some of the pore constrictions were dislodged at higher hydrodynamic forces. This behavior is similar to the effect of higher hydrodynamic forces on colloid release from grain surfaces (Torkzaban et al., 2007, 2008). It is expected that the difference in the pore-size distribution between cores 466 and 555 would have an effect on hydrodynamic forces that contributed to the amount of hydrodynamic bridging, colloid release, and the associated dependence of permeability on v. Pore blockage caused by hydrodynamic bridging is expected to be more pronounced and persistent for smaller pore sizes.

3.3. Simulations

Figs. 3, 4, and 5 also show the simulated colloid release and permeability changes in cores 391, 555, and 466, respectively, by employing Eqs. (1)–(5). The fitted values of the model parameters for each step (i.e., solution chemistry and velocity increase) of the experiment are given in Table 3, along with the coefficient of linear regression (R^2). It should be acknowledged that parameter fits using the Levenberg–Marquardt algorithm in COMSOL may not always be unique because of the presence of local minima in the objective function. In an attempt to overcome this limitation, optimization was initiated several times with different initial parameter estimates, and the best result is shown in Figs. 3–5 and Table 3. Alternatively, global parameter optimization algorithms may also be employed (e.g., Vrugt et al., 2005). This is a topic of future study, but is beyond the scope of the current research.

Colloid release that was induced by a change in solution chemistry (Step A) was satisfactorily modeled using a first-order kinetic release expression (Eq. (3)) by accounting for the releasable fraction of colloid mass on the grain surfaces. The value of S_{i1} reflects the total initial amount of clay in the core and was set equal to 10, 50, and 50 g/kg in Step A for cores 391, 555, and 466, respectively, based on the XRD analyses. As mentioned earlier, values of S_{i1} for each subsequent release step (B1–B5) were obtained directly from the model output. The value of $(1 - f_{nr})$ in Step A presented in Table 3 indicates that only a small fraction of the in situ colloids was release when the IS was lowered to that of RO water in step A. The value of κ_1 was low, ranging from 0.000125 to 0.00055 s^{-1}, and may imply that reduction in the mean adhesive interaction with IS reduction occurred slowly and approached equilibrium conditions after many pore volumes of injection (>15 PVs). The release rate constant is frequently considered to be a diffusion controlled process that is a function of the diffusion coefficient and the boundary layer thickness (Ryan and Gschwend, 1994). However, this approach does not account for the kinetic reduction of the adhesive interactions due to the mass transfer kinetics of cations from the gap separating the deposited colloids and the collector surface (Bradford et al., 2014). Hydrodynamic bridging (colloid retention at the pore constrictions) was accounted for in the model using values of λ that ranged from 0.002 to 0.009 s^{-1}. Values of S_{max2} were optimized to determine the maximum amount of retained colloids at the pore throats necessary to render the retention coefficient of zero and ranged from 0.6 to 2 g/kg. In agreement with other reported studies (e.g., Khilar and Fogler, 1984; Kia et al., 1987), we found in another set of experiments (data not shown) that there is a critical salt concentration below which colloid release begins in cores from this aquifer. The critical ionic strength in the mixed salt groundwater used in this study was determined to be about 1.5 mM. It is noted that the first-order kinetic expression given in Eq. (3) was adequate to describe the dependency of colloid release on the solution IS during Step A.

A two-site kinetic model was needed to satisfactorily fit the sharp peak and long tail of the colloid release with changes in v. We, therefore, assumed that the amount of colloid release with increasing v could be divided into two types of retention sites.

One site involved the slow rate of release from the grain surfaces that continued for a long time before depletion. As mentioned above, the value of S_{i1} was large and reflects the initial amount of clay in the core. The second site accounted for the release of colloids from pore constrictions. A fast rate of release was needed to produce a sharp peak in the BTCs and quick depletion of the colloid mass from this second site. It was essential to estimate the value of f_{nr2} in Eq. (4), which is a fraction of colloids retained at pore constrictions released with an increase in v, in order to accurately capture the associated sharp permeability increase. In general, the value of κ_2 was more than one order of magnitude greater than that of κ_1. The peak value of the BTCs was mainly controlled by the values of κ_2 and f_{nr2}. A high value of κ_2 resulted in fast release until the total releasable colloid mass at the pore constrictions was exhausted. Consequently, a sudden increase in the permeability was predicted which was consistent with the observed permeability data. After the release curve begins its sharp fall due to exhaustion of releasable colloids from site 2 (pore constrictions), the shape of the release curve was mainly controlled by site 1 (release from the grain surfaces). At present, it is not possible to experimentally quantify the simultaneous colloid retention at and release from pore constrictions during flow alteration steps (B1–B5). Consequently, the simulated release rate during Steps B1–B5 reflects a net effect of retention and release. As a result, the value of λ was set to zero in these steps. This assumption is further justified by the negligible permeability reduction during these steps.

One would expect that Eq. (5) with a single value of β for a given core sample should be able to reproduce the observed permeability increases following the increase of flow velocity in Steps B1–B5. However, the value of β needed to be optimized at different flow velocities for the core samples of 555 and 466 in order to reproduce the observed permeability increases. This likely reflects that colloids were liberated from bridges have various pore throat sizes at different velocities. In particular, colloid bridges at larger pore throats are expected to be eliminated at a lower hydrodynamic force and flow rate (e.g., Steps B1 and B2) than bridges at smaller pore throats. As such, the permeability increase was high at the initial steps of flow velocity increase. However, when the flow velocity was further increased, the excessive hydrodynamic force caused remobilization of colloid bridges at some of the smaller pore throats which resulted in a smaller permeability increase.

4. Conclusions

Changing solution chemistry from a low salinity (35 mS/m) groundwater with both sodium and calcium present to reverse-osmosis water resulted in significant release of colloids originally deposited on sandstone core material. However, mass balance information indicated that only a relatively small fraction (<16%) of the deposited colloids were released, and that the majority of in situ colloids were held in a deep primary energy minimum in the presence of the native groundwater. This colloidal release resulted in a 60–70% reduction in aquifer permeability for cores with kaolinite content 6.1–7.4%, but no permeability reduction was observed for sandstone with 1.3% kaolinite. For the core samples tested it was demonstrated that the primary mechanism of clogging was hydrodynamic bridging of released colloids at pore constrictions when the IS was decreased. The importance of flow velocity and interruptions on colloid release and improvements in the core permeability were demonstrated.

It is also clear from our modeling and experiments that the deliberate increase in velocity, as would occur during injection well rehabilitation procedures such as backwashing or air-development, may increase permeability. That is, appropriate and early injection well rehabilitation strategies designed to alter the torque and forces acting on the colloids may prove effective in mitigating clogging induced by colloid release resulting from introduction of low solute concentration water. A further and significant finding from our research is that flow interruption which allows colloids to diffuse out of a pore constriction is potentially effective in reducing the impact of hydrodynamic bridging and may further remediate clogging.

Acknowledgments

This work was supported by the Water Corporation of Western Australia and the Gas Industry Social and Environmental Research Alliance (GISERA). GISERA is a collaborative vehicle established by CSIRO and Australia Pacific LNG to undertake publicly reported research addressing the socio-economic and environmental impacts of Australia's natural gas industries. For more details about GISERA visit www.gisera.org.au. All data can be provided upon request from the corresponding author.

References

Adamczyk, Z., Siwek, B., Szyk, L., 1995. Flow-induced surface blocking effects in adsorption of colloid particles. J. Colloid Interface Sci. 174, 130–141.
Bacchin, P., Derekx, Q., Veyret, D., Glucina, K., Moulin, P., 2013. Clogging of microporous channels networks: role of connectivity and tortuosity. Microfluid. Nanofluid. 1–12.
Bedrikovetsky, P., Zeinijahromi, A., Siqueira, F.D., Furtado, C., de Souza, A.L.S., 2012. Particle detachment under velocity alternation during suspension transport in porous media. Transp. Porous Media 91 (1), 173–197.
Bergendahl, J., Grasso, D., 2000. Prediction of colloid detachment in a model porous media: hydrodynamics. Chem. Eng. Sci. 55 (9), 1523–1532.
Blume, T., Weisbrod, N., Selker, J.S., 2002. Permeability changes in layered sediments: impact of particle release. Ground Water 40, 466–474.
Bradford, S.A., Torkzaban, S., 2012. Colloid adhesive parameters for chemically heterogeneous porous media. Langmuir 28, 13643–13651.
Bradford, S.A., Torkzaban, S., 2013. Colloid interaction energies for physically and chemically heterogeneous porous media. Langmuir 29, 3668–3676.
Bradford, S.A., Torkzaban, S., Wiegmann, A., 2011. Pore-scale simulations to determine the applied hydrodynamic torque and colloid immobilization. Vadose Zone J. 10, 252–261.
Bradford, S.A., Torkzaban, S., Kim, H., Simunek, J., 2012. Modeling colloid and microorganism transport and release with transients in solution ionic strength. Water Resour. Res. 48, W09509. http://dx.doi.org/10.1029/2012WR012468.
Bradford, S.A., Torkzaban, S., Shapiro, A., 2013. A theoretical analysis of colloid attachment and straining in chemically heterogeneous porous media. Langmuir 29 (6944-2952).
Bradford, S.A., Wang, Y., Kim, H., Torkzaban, S., Šimůnek, J., 2014. Modeling microorganism transport and survival in the subsurface. J. Environ. Qual. 43 (2), 421–440.
Bradford, S.A., Torkzaban, S., Leij, F., Simunek, J., 2015a. Equilibrium and kinetic models for colloid release under transient solution chemistry conditions. J. Contam. Hydrol. 181, 141–152.
Bradford, S.A., Wang, Y., Torkzaban, S., Šimůnek, J., 2015b. Modeling the release of *E. coli* D21g with transients in water content. Water Resour. Res. http://dx.doi.org/10.1002/2014WR016566.
Chrysikopoulos, C.V., Syngouna, V.I., 2014. Effect of gravity on colloid transport through water-saturated columns packed with glass beads: modeling and experiments. Environ. Sci. Technol. 48, 6805–6813.

Derjaguin, B.V., Landau, L.D., 1941. Theory of the stability of strongly charged lyophobic sols and of the adhesion of strongly charged particles in solutions of electrolytes. Acta Physicochim. U.S.S.R. 14, 733–762.
Dillon, P., Pavelic, P., Massmann, G., Barry, K., Correll, R., 2001. Enhancement of the membrane filtration index (MFI) method for determining the clogging potential of turbid urban stormwater and reclaimed water used for aquifer storage and recovery. Desalination 140 (2), 153e165.
Duffadar, R.D., Davis, J.M., 2007. Interaction of micrometer-scale particles with nanotextured surfaces in shear flow. J. Colloid Interface Sci. 308, 20–29.
Goldenberg, L.C., Magaritz, M., Amiel, A.J., Mandel, S., 1984. Changes in hydraulic conductivity of laboratory sand clay mixtures caused by a seawater freshwater-interface. J. Hydrol. 70, 329–336.
Grolimund, D., Borkovec, M., 2006. Release of colloidal particles in natural porous media by monovalent and divalent cations. J. Contam. Hydrol. 87, 155–175.
Grolimund, D., Borkovec, M., Barmettler, K., Sticher, H., 1996. Colloid facilitated transport of strongly sorbing contaminants in natural porous media: a laboratory column study. Environ. Sci. Technol. 30, 3118–3123.
Grolimund, D., Elimelech, M., Borkovec, M., Barmettler, K., Kretzschmar, R., Sticher, H., 1998. Transport of in situ mobilized colloidal particles in packed soil columns. Environ. Sci. Technol. 32, 3562–3569.
Grolimund, D., Barmettler, K., Borkovec, M., 2001. Release and transport of colloidal particles in natural porous media 2. Experimental results and effects of ligands. Water Resour. Res. 37, 571–582.
Grosberg, A.Y., Nguyen, T.T., Shklovskii, B.I., 2002. Colloquium: the physics of charge inversion in chemical and biological systems. Rev. Mod. Phys. 74 (2), 329.
Khilar, K.C., Fogler, H.S., 1984. The existence of a critical salt concentration for particle release. J. Colloid Interface Sci. 101, 214–224.
Khilar, K., Fogler, S., 1998. Migration of Fines in Porous Media. Kluwer Academic Publishers, Dordrecht.
Kia, S.F., Fogler, H.S., Reed, M.G., Vaidya, R.N., 1987. Effect of salt composition on clay release in Berea sandstones. SPE Prod. Eng. 2, 277–283.
Konikow, L.F., August, L.L., Voss, C.L., 2001. Effects of clay dispersion on aquifer storage and recovery in coastal aquifers. Transp. Porous Media 43, 45–64.
Kuznar, Z.A., Elimelech, M., 2007. Direct microscopic observation of particle deposition in porous media: role of the secondary energy minimum. Colloids Surf. A 294, 156–162.
Clogging Issues Associated With Managed Aquifer Recharge Methods. IAH Commission on Managing Aquifer Recharge. In: Martin, R. (Ed.), (www.iah.org/recharge/clogging.htm).
Mays, D., Hunt, J., 2005. Hydrodynamic aspects of particle clogging in porous media. J. Environ. Sci. Technol. 39 (2), 577–584.
Mondal, P.K., Sleep, B.E., 2012. Colloid transport in dolomite rock fractures: effects of fracture characteristics, specific discharge, and ionic strength. Environ. Sci. Technol. 46 (18), 9987–9994.
Ochi, J., Vernoux, J.F., 1998. Permeability decrease in sandstone reservoirs by fluid injection: hydrodynamic and chemical effects. J. Hydrol. 208, 237–248.
Pavelic, P., Dillon, P.J., Barry, K.E., Vanderzalm, J.L., Correll, R.L., Rinck-Pfeiffer, S.M., 2007. Water quality effects on clogging rates during reclaimed water ASR in a carbonate aquifer. J. Hydrol. 334, 1e16.
Ramachandran, V., Fogler, H.S., 1999. Plugging by hydrodynamic bridging during flow of stable colloidal particles within cylindrical pores. J. Fluid Mech. 385, 129–156.
Ramachandran, V., Venkatesan, R., Tryggvason, G., Fogler, S.H., 2000. Low Reynolds number interactions between colloidal particles near the entrance to a cylindrical pore. J. Colloid Interface Sci. 229 (2), 311–322.
Rosenbrand, E., Fabricius, I., Yuan, H., 2012. Thermally induced permeability reduction due to particle migration in sandstones: the effect of temperature on kaolinite mobilisation and aggregation. Proceedings of 37th Workshop on Geothermal Reservoir Engineering. Stanford University, Stanford, California (January 30–February 1).
Roy, S.B., Dzombak, D.A., 1996. Colloid release and transport processes in natural and model porous media. Colloids Surf. A Physicochem. Eng. Asp. 107, 245–262.
Ryan, J.N., Elimelech, M., 1996. Colloid mobilization and transport in groundwater. Colloids Surf. A Physicochem. Eng. Asp. 107, 1–56.
Ryan, J.N., Gschwend, P.M., 1994. Effects of ionic-strength and flow-rate on colloid release — relating kinetics to intersurface potential-energy. J. Colloid Interface Sci. 164, 21–34.
Salama, R.B., 2005. Interconnectivity between the superficial aquifer and the deep confined aquifers on the Gnangara Mound, Western Australia. Water Air Soil Pollut. Focus 5, 27–44. http://dx.doi.org/10.1007/s11267-005-7395-9.
Sasidharan, S., Torkzaban, S., Bradford, S.A., Dillon, P.J., Cook, P.G., 2014. Coupled effects of hydrodynamic and solution chemistry on long-term nanoparticle transport and deposition in saturated porous media. Colloids Surf. A Physicochem. Eng. Asp. 457, 169–179.
Seibert, S., Prommer, H., Siade, A., Harris, B., Trefry, M., Martin, M., 2014. Heat and mass transport during a groundwater replenishment trial in a highly heterogeneous aquifer. Water Resour. Res. 1944–7973.
Shen, C., Li, B., Huang, Y., Jin, Y., 2007. Kinetics of coupled primary- and secondary-minimum deposition of colloids under unfavorable chemical conditions. Environ. Sci. Technol. 41, 6976–6982.
Shen, C., Lazouskaya, V., Zhang, H., Wang, F., Li, B., Jin, Y., Huang, Y., 2012. Theoretical and experimental investigation of detachment of colloids from rough collector surfaces. Colloids Surf. A Physicochem. Eng. Asp. 410, 98–110.
Syngouna, I.V., Chrysikopoulos, C.V., 2015. Experimental investigation of virus and clay particles cotransport in partially saturated columns packed with glass beads. J. Colloid Interface Sci. 440 (15), 140–150.
Torkzaban, S., Bradford, S.A., Walker, S.L., 2007. Resolving the coupled effects of hydrodynamics and DLVO forces on colloid attachment to porous media. Langmuir 23, 9652–9660.
Torkzaban, S., Tazehkand, S.S., Walker, S.L., Bradford, S.A., 2008. Transport and fate of bacteria in porous media: coupled effects of chemical conditions and pore space geometry. Water Resour. Res. 44, W04403. http://dx.doi.org/10.1029/2007WR006541.
Torkzaban, S., Hyunjung, N.K., Simunek, J., Bradford, S.A., 2010. Hysteresis of colloid retention and release in saturated porous media during transients in solution chemistry. Environ. Sci. Technol. 44, 1662–1669.
Torkzaban, S., Wan, J., Tokunaga, T.K., Bradford, S.A., 2012. Impacts of bridging complexation on the transport of surface-modified nanoparticles in saturated sand. J. Contam. Hydrol. 136–137, 86–95.
Torkzaban, S., Bradford, S.A., Wan, J., Tukunaga, T., Masoudih, A., 2013. Release of quantum dot nanoparticles in porous media: Role of cation exchange and aging time. Environ. Sci. Technol. 47, 11528–11536.
Tosco, T., Tiraferri, A., Sethi, R., 2009. Ionic strength dependent transport of microparticles in saturated porous media: modeling mobilization and immobilization phenomena under transient chemical conditions. Environ. Sci. Technol. 43, 4425–4431.
Vasiliadou, I.A., Chrysikopoulos, C.V., 2011. Cotransport of *Pseudomonas putida* and kaolinite particles through water-saturated columns packed with glass beads. Water Resour. Res. 47, W02543. http://dx.doi.org/10.1029/2010WR009560.
Verwey, E.J.W., Overbeek, J.Th.G., 1948. Theory of the Stability of Lyophobic Colloids. Elsevier, Amsterdam.
Vrugt, J.A., Diks, C.G.H., Gupta, H.V., Bouten, W., Verstraten, J.M., 2005. Improved treatment of uncertainty in hydrologic modeling: Combining the strengths of global optimization and data assimilation. Water Resour. Res. 41, 1. http://dx.doi.org/10.1029/2004WR003059.
Wiesner, M.R., Grant, M.C., Hutchins, S.R., 1996. Reduced permeability in groundwater remediation systems: role of mobilized colloids and injected chemicals. Environ. Sci. Technol. 30, 3184–3191.
Yao, K.-M., Habibian, M.T., O'Melia, C.R., 1971. Water and waste water filtration: concepts and applications. Environ. Sci. Technol. 5, 1105–1112.
Zeinijahromi, A., Lemon, P., Edrikovetsky, P., 2011. Effects of induced migration of fines on water cut during waterflooding. J. Pet. Sci. Eng. 78, 609–617.
Zhou, J., Zheng, X., Flury, M., Lin, G., 2009. Permeability changes during remediation of an aquifer affected by sea-water intrusion: a laboratory column study. J. Hydrol. 376, 557–566.